[논 문] 한국재료학회지
Korean J. Mater. Res.
Vol. 28, No. 10 (2018)
https://doi.org/10.3740/MRSK.2018.28.10.551

Transparent Ceramics for Visible/IR Windows: Processing, Materials and Characterization

Wook Ki Jung[1], Ho Jin Ma[1], Ha-Neul Kim[2†] and Do Kyung Kim[1†]

[1]Department of Materials Science and Engineering, Korea Advanced Institute of Science and Technology (KAIST), 291 Daehak-ro, Yuseong-gu, Daejeon 34141, Republic of Korea
[2]Engineering Ceramics Research Group, Korea Institute of Materials Science, 797 Changwon-daero, Changwon 51508, Republic of Korea

(Received August 3, 2018 : Revised September 20, 2018 : Accepted September 20, 2018)

Abstract Visible and IR windows require a combination of high optical transparency and superior thermal and mechanical properties. Materials, fabrication and characterization of transparent ceramics for visible/IR windows are discussed in this review. The transparent polycrystalline Y_2O_3, Y_2O_3-MgO nanocomposites and $MgAl_2O_4$ spinel ceramics are fabricated by advanced ceramic processing and the use of special sintering technologies. Ceramic processing conditions for achieveing fully densified transparent ceramics are strongly dependent on the initial powder characteristics. In addition, appropriate use of sintering technologies, including vacuum sintering, hot-pressing and spark plasama sintering methods, results in outstanding thermal and mechanical properties as well as high optical transparency of the final products. Specifically, the elimination of light scattering factors, including residual pores, second phases and grain boundaries, is a key technique for improving the characteristics of the transparent ceramics. This paper discusses the current research issues related to synthesis methods and sintering processes for yttria-based transparent ceramics and $MgAl_2O_4$ spinel.

Key words transparent ceramics, visible/IR windows, ceramic processing, characterization.

1. Introduction

Conventional optical transparent materials including glasses and polymers offer limited use in window applications requiring high thermal and mechanical properties. Single crystals meet the requirements, but fabricating large-scale single crystals is relatively difficult and time-consuming. With the advancement of ceramic technologies, transparent ceramics garnering interest for visible/IR windows employed in harsh and extreme environments.[1-5)]

The theoretical transparency of ceramics is determined by the inherent material refractive index(n), which is a function of light wavelength. Optically transparent ceramics from the visible to IR wavelength range are promising candidates for visible/IR window applications.[3,6)] Transparent ceramics can be obtained theoretically by eliminating the light scattering and absorption factors considering the Beer-Lambert law.[7)] Light scattering is an important factor as it decreases the transmittance of ceramics exponentially, and can be separated into three different origins: (1) grain boundary scattering, (2) pore scattering and (3) impurity scattering. Light scattering at the grain boundary, which does not exist in a cubic crystal structure, can occur in polycrystalline ceramics with a non-cubic structure.[8,9)] The impurity phase in the transparent ceramics can cause light scattering depending on the difference in the refractive index between the host and impurity. The most significant scattering factor is porosity, considering the refractive index of the air. Mie scattering theory indicates that even a very small amount of porosity in the microstructure significantly deteriorates light transmittance, especially from the visible to IR range.[8)] In this regard, the strategy of pore elimination is crucial for the fabrication of transparent ceramics.

The fabrication of transparent polycrystalline ceramics is strongly dependent on ceramic processing and sintering

†Corresponding author
E-Mail : skykim@kims.re.kr (H.-N. Kim, KIMS)
dkkim@kaist.ac.kr (D. K. Kim, KAIST)

technologies. Numerous studies on ceramic window candidates, Y_2O_3, Y_2O_3-MgO nanocomposites, and $MgAl_2O_4$ spinel, have been carried out. Ceramic processing of powder preparation strategies, shaping and special sintering processes has been demonstrated to overcome the challenging issues. The pore elimination process depends largely on microstructure control such as control over the grain growth kinetics and pore characteristics. Excessive grain growth during densification causes pore trapping in the grains, and it is very difficult to remove closed pores compared to open pores.[10,11)]

Sintering additives can control the grain growth behavior and densification. The grain growth inhibitors operate as chemical defects or 'pinning effects' to suppress grain boundary migration. The doping of tetravalent ions causes yttrium interstitial defects in Y_2O_3 ceramics, which decrease the grain growth rate during sintering.[12)] Beyond the solubility limit of MgO in Y_2O_3, the magnesia phase effectively inhibits grain growth by pinning the grain boundaries, thereby enabling the fabrication of fully densified Y_2O_3-MgO nanocomposites.[13)] Several sintering aids are used for liquid phase formation to allow densification of $MgAl_2O_4$ without excessive grain growth at relatively low temperature.[14-16)] A small amount of co-additives is known to reduce the intergranular pores in transparent ceramics.

The use of special sintering technologies is required for the processing of transparent ceramics. A vacuum sintering process is preferred to extract the nitrogen gas from the pellets. Hot-press(HP) and spark plasma sintering(SPS) densify ceramics at relatively low temperature and short time, inhibiting excessive grain growth. Fine grained transparent ceramics can be obtained with the combination of optimized pre-sintering and a subsequent hot isostatic pressing(HIP) procedure. A post-annealing process refills the oxygen vacancies, which are generated during sintering in a reducing atmosphere, and eliminate the carbon contamination in the final products.

In this paper, recent ceramic processing and characterization of visible/IR transparent ceramics is reviewed. Detailed fabrication procedures are described focusing on minimizing light scattering factors. The optical and thermomechanical properties are also discussed for promising ceramic window candidates.

2. Ceramic Processing

2.1 Powder preparation and processing

The characteristics of starting powders affect the sintering behavior and optical properties of transparent ceramics. Ceramic powder should be prepared considering particle size, uniformity, purity, calcinations, and proper additives for sintering. Particle size and uniformity affect the characteristics of green body homogeneity. The powder purity has a critical influence on the optical absorption loss of the final sintered body. Sintering additives are used for pore elimination and densification during sintering at high temperature.

High purity powder(> 99.99 %) is preferred for fabrication of transparent ceramics. The commercial powder can be further purified by various chemical methods to obtain high quality transparent ceramics. Kim et al.[1,17-19)] at NRL fabricated exit window materials with a low absorption coefficient in a high energy laser system by using acid-washed powders. High-purity powder can also be synthesized by a chemical synthesis route with high purified precursors. The high-purity powders are also synthesized by a co-precipitation method using high-purity chlorides, nitrates or carbonates precursors.[20-24)] In some cases, the powders are dissolved in hot acid followed by recrystallization to obtain high purity precursors prior to synthesis.[18,25)]

The particle size and distribution can be controlled by choosing relevant synthesis parameters such as pH, temperature, time, and calcination.[22,26)] It is known that strong agglomerates of starting particles easily induce intragranular pores due to an abnormal grain growth and make it difficult to obtain zero porosity microstructure. The particle size and distribution is optimized to achieve the desired homogeneous microstructure and high sinterability.[27,28)] The effect of the calcination conditions on the as-synthesized powders, the microstructure of sintered body, and their optical transmittance have been reported.[29,30)] The calcination temperature and atmosphere of the powders are related to particle agglomeration, crystallite size, and particle density, which affect the pore elimination procedure during sintering.

Sintering aids alleviate the severe sintering conditions required to eliminate residual pores. By adding some sintering aids into the powders, the inhibition of grain growth is expected during a densification.[16,31-34)] The grain growth kinetics strongly affects the pore elimination. Therefore, grain growth inhibitors are generally used for the fabrication of transparent ceramics. The influence of various dopants on the grain growth of sesquioxides has been systematically investigated.[31,35,36)] The defect mechanism and dopant effects have been studied, where oxygen vacancies are known to promote grain growth. Other sintering additives have been examined to form a liquid phase for an accelerated densification. The fabrication of transparent $MgAl_2O_4$ by adding CaO, B_2O_3, TiO_2, SiO_2, LiF, and various fluorides and chlorides for liquid phase formation has been reported.[14,15,37-39)] After the liquid phase sintering, the residual secondary phase can deteriorate optical transmittance.[40)]

The techniques for forming a green body can be

classified into two types. One is a dry process and the other is a wet process. The dry process includes powder granulation, pelletizing by a uniaxial press under pressure, and cold isostatic press(CIP). The wet process involves various consolidation methods such as freeze granulation, gel-casting, slip-casting and tape-casting.[34,40-45] It is noteworthy that the slip can be contaminated by molds such as Al_2O_3 and gypsum. The contaminated slip can change the sintering behavior and final microstructure and light transmittance of transparent ceramics.[40] The optimum granulation and compaction process influenced the homogeneity of green body and microstructure of the sintered body.[46,47]

2.2 Sintering technologies

2.2.1 Vacuum sintering

The processing of transparent ceramics requires special sintering technologies to obtain optical transparency. Vacuum sintering can be employed to eliminate nitrogen gas from the ceramics because nitrogen is difficult to be extracted under atmospheric pressure.[48] It has been typically used for sintering of transparent sesquioxides including Y_2O_3, Yb_2O_3, Sc_2O_3, and Lu_2O_3 ceramics.[49-51] Fully dense polycrystalline sesquioxides are typically obtained in a vacuum graphite furnace or a tungsten mesh-heated vacuum furnace under 10^{-6} Torr at 1,800 °C. Coarse average grain size from tens to hundreds of micrometers is obtained after vacuum sintering. Excessive grain growth during vacuum sintering can cause pore trapping in the grains. For this reason, the addition of a grain growth inhibitor is required in the powder preparation step.

The vacuum atmosphere induces oxygen vacancies in the sintered products, resulting in black colored specimens, or so-called discoloration. A post-annealing procedure is required to replenish the oxygen ion after vacuum sintering.[52,53] As shown in Fig. 1, as-sintered 3.0 at. % Yb:LuAG transparent ceramics has oxygen vacancies, which induce broad absorption bands in visible region. After annealing process in air condition, the oxygen vacancy can be removed that the transmittance is improved in the visible region, and the ceramics become colorless.[54] It is known that the post-annealing inevitably induces pore development, and this decreases optical transmittance. To solve this problem, a further hot isostatic pressing(HIP) is used after post-annealing in air for a long time.[55,56]

2.2.2 Hot-press(HP)

A hot-press is an equipment to sinter by applying pressure to make a powder mixture or a green body fully dense at relatively low temperature. As illustrated in Fig. 2, the facility is composed of a graphite furnace and a

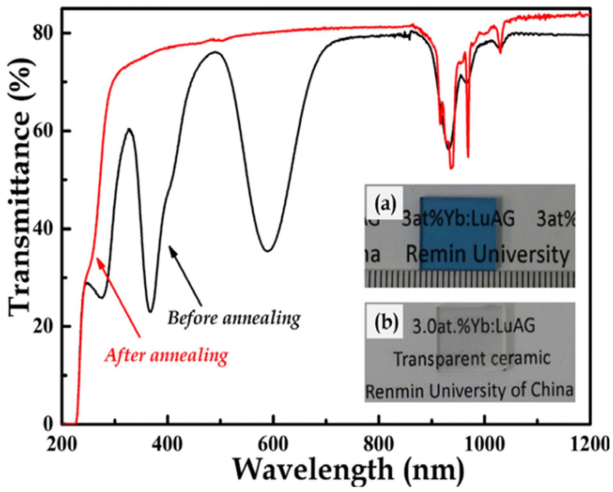

Fig. 1. Transmittance spectra of 3 at. % Yb-doped LuAG transparent ceramics. Inset shows the picture of (a) as-sintered in vacuum and (b) annealed ceramics. Reproduced with permission from Ref.,[54] Copyright 2016. John Wiley & Sons.

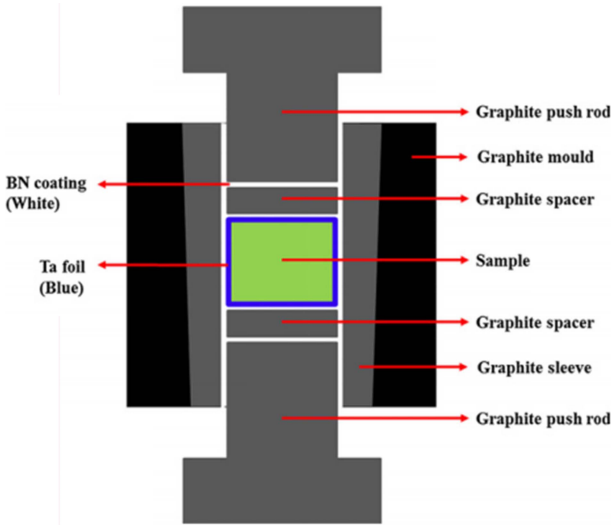

Fig. 2. Schematic diagram of the hot-pressing arrangement. Reproduced with permission from Ref.,[57] Copyright 2015, John Wiley & Sons.

graphite uniaxial press die, and operates mainly in an argon gas or vacuum atmosphere.[57] A post-annealing procedure is required to remove carbon contamination and fulfill oxygen ion after application of the HP method. A further HIP process can be used to increase the transmittance very close to the theoretical value.[57] The optimization of sintering parameters, including temperature and pressure schedule, is necessary.

In addition to grain boundary and volume diffusion, the plastic deformation and creep process are also important sintering mechanisms when applying high pressure. It is

effective when the grain growth rate is faster than the densification speed. Since the densification driving force is increased, the sintering time can be shortened, which further suppresses grain growth significantly. For this reason, fully dense ceramics with effectively inhibited grain size can be obtained. The transparent ceramics including Y_2O_3, Y_2O_3-MgO nanocomposite, and $MgAl_2O_4$ spinel are sintered via the HP method.[58-60] It has been reported that transparent Y_2O_3 ceramics can be fabricated at the low temperatures(1,600 °C) and 20 MPa of pressure under a vacuum of 9×10^{-3} Pa.[57,60] Small grain size(~1 μm) was obtained, and high transparency with full density was reported. HP has also been reported to produce Y_2O_3-MgO nanocomposites with high mechanical properties and infrared transmittance.[61] Hot-pressed Y_2O_3-MgO nanocomposites were highly transparent in the region of infrared wavelengths(1-9 μm). The final small grain size(~100 nm) resulted in a high mechanical strength of the ceramics. Transparent $MgAl_2O_4$ spinel has also been obtained at low temperature(1,600 °C) under pressure (< 50 MPa) via HP.[62,63]

2.2.3 Spark plasma sintering(SPS)

Spark plasma sintering(SPS) realizes fully dense transparent ceramics with fine grains because of its low temperature and short sintering time. It is also called the field assisted sintering technique(FAST) or pulsed electric current sintering(PECS).[64,65] The SPS is a technique to densify nanopowders with the aid of pulsed DC current at a low temperature under pressure. Unlike the case of the HP or conventional sintering equipment where heat is generated from an external heating element, the pulsed DC current of SPS directly passes through ceramic powders in a graphite die, to generate a Joule heating in the samples. Fast consolidation takes place through the pulsed DC current for a short period of time(within minutes), to limit grain growth, that is, a very small size. The advantage of the inhibition of grain growth reduce the grain size is to produce not only oxide ceramics of the cubic structure but also non-cubic ceramics with a transparency.[10,66] Transparent ceramics fabricated by using SPS including Y_2O_3, Y_2O_3-MgO, and $MgAl_2O_4$ have been widely investigated.[67-70] The discoloration of $MgAl_2O_4$ spinel has been studied via the use of SPS. The discoloration was found to be due to carbon contamination and lattice defects depending on the SPS operating conditions. Recently, Morita et al.[67,68] investigated the discoloration phenomenon of SPS sintered $MgAl_2O_4$ spinel and reported that the heating rate influences the discoloration originating from lattice defects as well as pore generation. As shown in Fig. 3, The heating rate and holding time are the most important sintering parameters for the fabrication of transparent ceramics in the case of SPS.[71] Rapid densification of SPS generates dislocations, which results in black colored sample. From the analyses of Raman spectra and ERS, it appears that the evaporated carbon from the graphite paper/die easily enters the samples through open pore channels under a rapid heating rate.

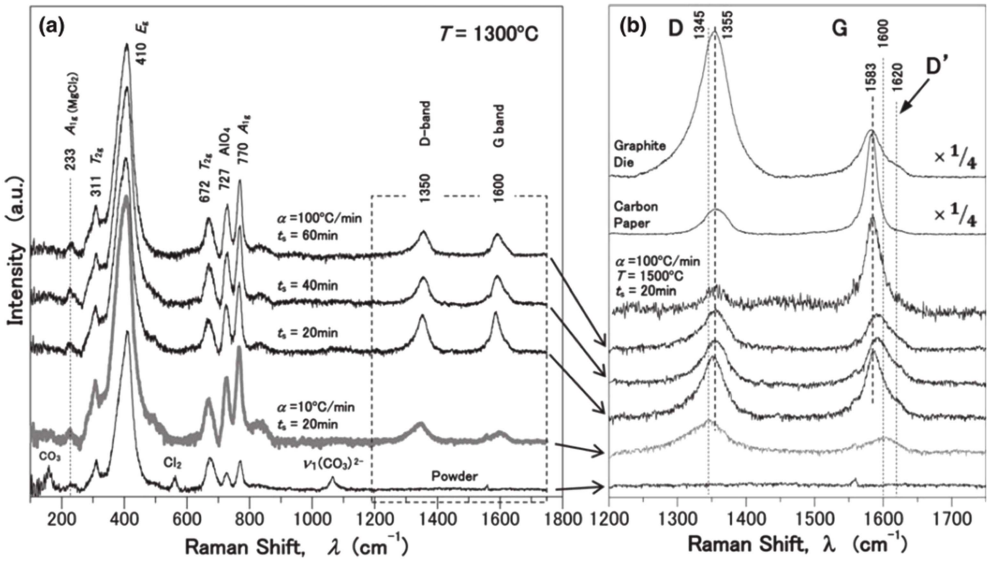

Fig. 3. (a) Raman spectra of the $MgAl_2O_4$ spinel sintered by SPS at 1,300 °C for 20 to 60 min with different heating rate between 10 and 100 °C/min. (b) Enlarged Raman spectra indicated by broken line(1,200-1,750 cm^{-1}) in (a). For comparison, the Raman spectra of the starting powder, the carbon paper and graphite die, and the spinel at T = 1,500 °C for 20 min with heating rate of 100 °C/min are also shown. Reproduced with permission from Ref.,[71] Copyright 2015, John Wiley & Sons.

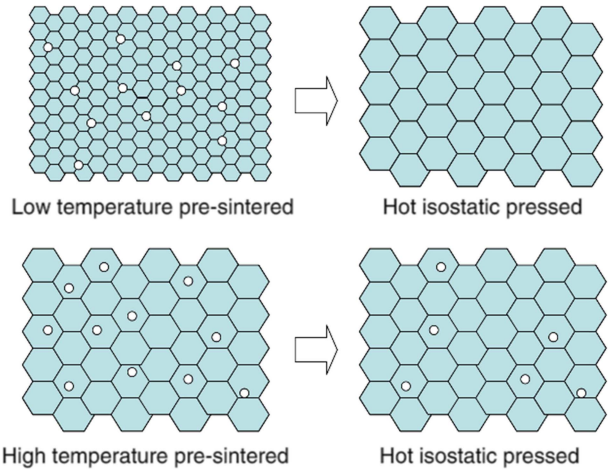

Fig. 4. Schematic of microstructure for pore elimination by hot isostatic pressing. Reproduced with permission from Ref.,[78] Copyright 2008, John Wiley & Sons.

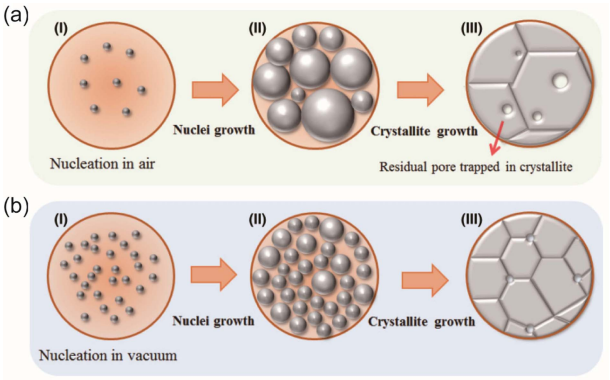

Fig. 5. Schematic of nucleation, nuclei growth, and relevant pores of spherical Y_2O_3 particles during crystallization (a) in air (b) and under vacuum, respectively, Residual pores are trapped in a bigger crystallite in an air atmosphere(A-III), Smaller crystallites and intergranular pores remained in the vacuum atmosphere(B-III), Reproduced with permission from Ref.,[30] Copyright 2017, John Wiley & Sons.

2.2.4 Hot isostatic pressing(HIP)

Hot isostatic pressing(HIP) is used to reduce residual pores of transparent ceramics and to achieve a maximum density. It is an important procedure to achieve high-end optical transmitting ceramics. An isostatic gas pressure is applied in the chamber during high temperature sintering. Because the post-annealed samples still contain residual pores, the HIP procedure is introduced at the last stage to make a pore-free microstructure.[55,72-74] The residual pores in pre-sintered ceramics can also be completely removed through the use of HIP equipment. The pre-sintering and following HIP procedure is advantageous for improving mechanical strength owing to the fine microstructure with the submicrometer grain size.[11,75,76] The optical transmittance of hot isostatically pressed(HIPed) samples is strongly affected by the pre-sintering temperature and conditions. As shown in Fig. 4, it is known that the intragranular pores generated by excessive grain growth are difficult to remove in the HIP stage.[11,77,78] Therefore, it is important to densify the pre-sintered ceramics without generating intragranular pores to make transparent ceramics. Transparent Y_2O_3 and $MgAl_2O_4$ spinel can be fabricated by pre-sintering(vacuum sintering, pressureless sintering, HP, SPS) and subsequent HIP.[15,56,57,74,79,80]

3. Materials and Characterization

3.1 Y_2O_3 optical ceramics

Yttria(Y_2O_3) ceramics exhibit superior optical properties, such as long wavelength cut-off(> 5 μm) and low IR emissivity at a high temperature in comparison to those of the other transparent ceramics.[5] Therefore, Y_2O_3 ceramics are an attractive candidate for practical applications, especially for IR windows. The Y_2O_3 transparent ceramic has a cubic crystal structure showing no birefringence in the polycrystalline ceramics.[81] The residual porosity is the most significant cause of optical transmittance decay. The ceramic processing and special sintering technologies have been reported the effective pore elimination in Y_2O_3 ceramics.[82,83]

Highly sinterable powder is favored to make transparent Y_2O_3 ceramics because it decreases the sintering temperature for densification. Ikegami et al. synthesized low-agglomerated powder from carbonates and fabricated transparent Y_2O_3 ceramics at a relatively low temperature.[22] The low-agglomerated powder exhibits homogeneous microstructure, preventing an abnormal grain growth. It was reported that the low temperature synthesis of sulfate-doped Y_2O_3 produced a well dispersed morphology of the Y_2O_3 powder.[20,84,85] The characteristics of as-synthesized powder can be changed through the calcination conditions such as temperature and atmosphere.[29,30] Jung et al. reported the influence of the calcination atmosphere on the crystallite size of powders, particle density, and the optical transmittance of sintered Y_2O_3 ceramics.[30] The smaller crystallites of powder enhance the elimination of closed pores in the particles at higher calcination temperature, resulting in a highly densified powder, as represented in Fig. 5. A starting powder with high density is advantageous for the pore elimination step during the sintering procedure.

Sintering aids for liquid phase sintering of Y_2O_3 have been employed for low temperature sintering in past decades. The formation of liquid phase is possible during sintering by using LiF, BeO, HfO_2, ThO_2, and La_2O_3.[86-90] The introduction of liquid phase to the microstructure is disadvantageous for the optical properties. Recently, grain

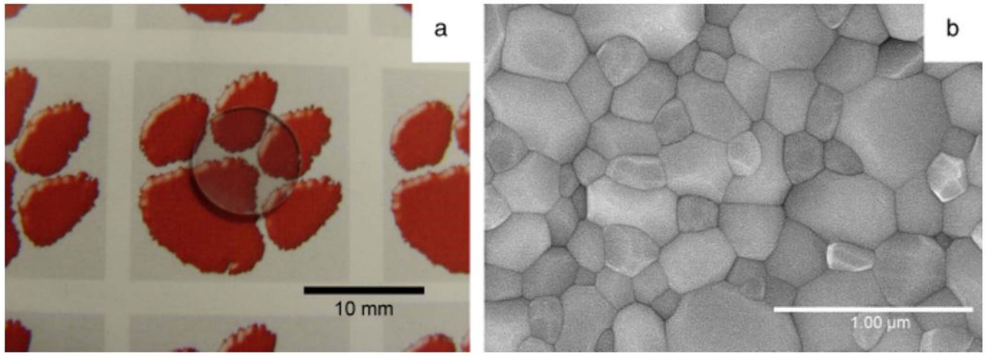

Fig. 6. (a) Optical image of the polished hot isostatically pressed(HIPed) Er-doped Y_2O_3 ceramic, (b) Scanning electron microscopy micrograph of the microstructure of the HIPed Er-doped Y_2O_3 ceramic, Reproduced with permission from Ref.,[94] Copyright 2010, John Wiley & Sons.

growth inhibitors are mainly used as additives in order to suppress pore trapping in the grains.[34,51,52,91,92]

The effect of ion doping on the grain growth kinetics and microstructure to fabricate transparent Y_2O_3 ceramics in vacuum sintering or a reduction atmosphere has been reported.[52,93] The yttrium interstitial defect, $[Y_i^{\cdots}]$, is the rate-controlling step for the grain boundary mobility of pure Y_2O_3. Since the grain boundary mobility of Y_2O_3 increases in a reducing atmosphere, an additive that inhibits the grain growth is needed to prevent the generation of closed pores induced by excessive grain growth. Chen et al.[12] investigated the grain boundary mobility in Y_2O_3 ceramics in a reducing atmosphere on the basis of the defect mechanism of divalent and tetravalent ions. The tetravalent ion acts as a donor that generates yttrium vacancy defects which restrain the grain growth. This is delineated as follows:

$$MO_2 \xrightarrow{Y_2O_3} 2M_Y' + 2O_o + O_i'', \; [O_i'']^{1.5} \propto [V_Y'''] \quad (1)$$

Jin et al. fabricated the Zr^{4+} doped transparent Y_2O_3 ceramics via slip casting and vacuum sintering. They studied the change of microstructure and optical transmittance according to the concentration difference of ZrO_2.[34] It was reported that the optimum doping concentration is less than 5 mol %, and exceeding 5 mol % causes excessive grain growth due to lattice distortion.

The relatively low mechanical strength of transparent Y_2O_3 is a critical issue for applications in extreme environments.[74] The fabrication procedure of transparent Y_2O_3 ceramics has been investigated to obtain high optical and mechanical properties to overcome this limitation. Reducing the grain size is one way to increase the mechanical strength according to the Hall-Petch relation. A two-step sintering approach and a subsequent HIP process can drastically reduce grain growth while achieving full density. Serivalsatit et al. reported highly

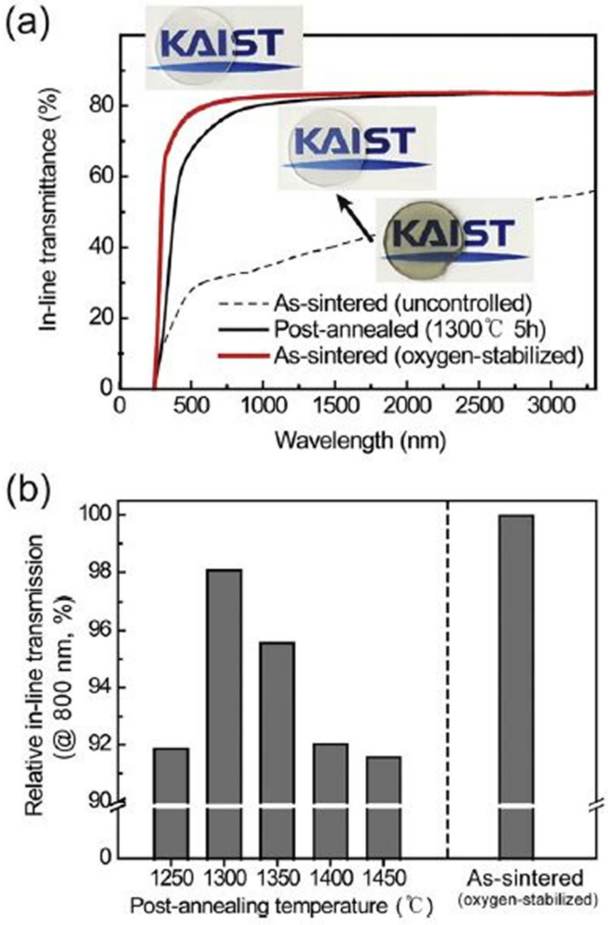

Fig. 7. (a) In-line transmittance of 1 mm-thick Y_2O_3 transparent ceramics, Inset: photographs of the corresponding samples, (b) In-line transmittance evaluated at λ = 800 nm (T_m, 800) of the oxygen-stabilized Y_2O_3 ceramics and post-annealed samples from 1,250 to 1,450 °C for 5h, respectively, Reproduced with permission from Ref.,[97] Copyright 2017, Elsevier.

transparent Y_2O_3 ceramics with submicrometer-grain size by optimizing the two-step sintering process.[75] As shown

in Fig. 6, they obtained average grain size of 300 nm, which improved the microhardness and fracture toughness of 1.39 MPa·$m^{1/2}$.[94] Kodo et al. reported the doping effect of various divalent cations on the two-step sintering of Y_2O_3 ceramics.[95] The literature implies that a further improvement of the mechanical properties is possible by the addition of dopants and the control of the microstructure. The use of a HP, a pressure-assisted technique, also has been introduced to reduce the grain size. Gan et al. fabricated highly transparent ceramics with fine microstructure via HP.[57] Many studies to obtain transparent monocrystalline Y_2O_3 specimens via the SPS method were reported.[70,96]

Post-annealing and a subsequent HIP process is required to remove the oxygen vacancies and carbon contamination generated during the sintering procedure in a vacuum or HP and SPS. Another facile fabrication of transparent Y_2O_3 ceramics has been reported for commercialization. Recently, a concept of wrapping the Y_2O_3 green body with tantalum foil was reported; this restricted the formation of oxygen vacancies as well as carbon contamination from the graphite mold during hot-pressing.[60] A facile approach to prepare transparent Y_2O_3 ceramics during vacuum sintering by stabilizing oxygen defects, as shown in Fig. 7, was reported.[97] The pore evolution during post-annealing of as-sintered Y_2O_3 ceramics was characterized. In addition, the problem of pore evolution by considering the thermodynamics and introducing Y_2O_3/ZrO_2 dual powder bed was successfully solved.

3.2 Y_2O_3-MgO nanocomposite

Outstanding thermal and mechanical properties of transparent ceramics are required for a reliable operation of IR windows in harsh environments. As a representative infrared transparent material, Y_2O_3 shows excellent optical properties in the infrared wavelength region, but has poor mechanical strength and thermal shock resistance. To overcome the drawbacks of Y_2O_3 transparent ceramics, submicron-grain transparent ceramics were studied by Raytheon in 2005.[98] When appropriate materials, especially MgO, constitute the nanocomposite with Y_2O_3 phase, fine grain size can be achieved by the Zener pinning effect at the grain boundaries. The nanocomposite has a high melting temperature and a stable state below the eutectic temperature with low mutual solubility. The Y_2O_3-MgO nanocomposite has the higher flexural strength and thermal shock resistance than the other polycrystalline transparent ceramics such as Y_2O_3 and $MgAl_2O_4$ spinel structure ceramics.[13] Regardless of the merits of this nanocomposite, applications are strictly restricted in the mid-IR region. The large difference in the refractive index between cubic MgO and Y_2O_3 induces significant grain boundary scattering,

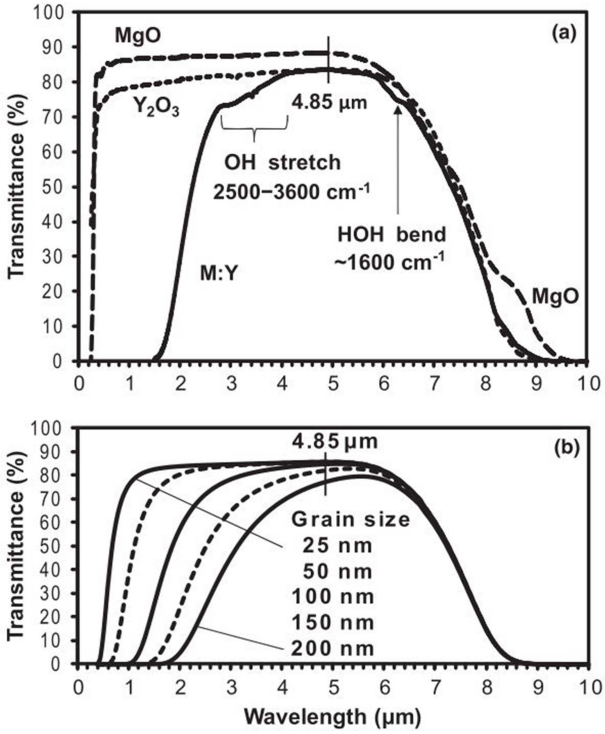

Fig. 8. (a) Transmission spectra of single crystal MgO, polycrystalline Y_2O_3(several-hundred-μm grain size), and M:Y, each with a thickness near 3.00 mm, (b) Predicted transmission of 3.00-mm-thick M:Y as a function of grain size, Reproduced with permission from Ref.,[13] Copyright 2013, John Wiley & Sons.

which deteriorates the near-IR transmittance. It is notable that the gran size of the nanocomposite should be limited below the wavelength of light to minimize the grain boundary scattering, as shown in Fig. 8. In this regards, the Y_2O_3-MgO nanocomposite is sintered at low sintering temperature by SPS,[69,99,100] HP,[58,101] and microwave sintering methods.[102,103]

When the Y_2O_3-MgO nanocomposite was introduced as a potential candidate for IR transparent ceramics in 2005, it had optical transmittance of 55 % at the mid-infrared region with average grain size of about 400 nm.[98] Wang et al fabricated a highly dense Y_2O_3-MgO nanocomposite using a high-temperature tube furnace at 1,400 °C, achieving high mid-infrared transparency of about 80 %. However, high sintering temperature brought about large grain size of 310 nm, which degraded the transmittance of short wavelength at 3 μm to 62 %.[104] It is crucial to prohibit domain coarsening. Jiang et al. synthesized the Y_2O_3-MgO nanoparticles via a sol-gel method. The nanopowder was then consolidated by the SPS technique.[69] As shown in Fig. 9, although the process is completed in an instant, the maximum transmittance above 80 % can be achieved, which is close to the theoretical transmittance at the mid-infrared region.

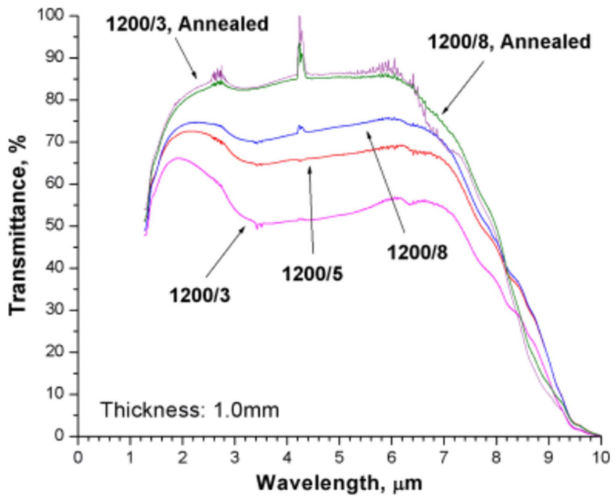

Fig. 9. Infrared transmittance of Y_2O_3-MgO nanocomposite consolidated by spark plasma sintering at 1,200 °C for different time. Influence of post-annealing is also represented. Reproduced with permission from Ref.,[69] Copyright 2010, John Wiley & Sons.

Huang et al. also studied the mechanical properties of Y_2O_3-MgO nanocomposite fabricated by the SPS method.[99] They produced fine domains from 125 to 223 nm under 100 MPa. They ascribed the grain growth of the Y_2O_3-MgO nanocomposite to grain boundary diffusion. In addition, the relation between microhardness and grain size followed the Hall-Petch equation.

Xu et al. fabricated a nanocomposite by glucose sol-gel synthesis and a HP sintering method.[58,105] HP was able to restrict the grain growth by applying pressure to the samples, similar to the SPS method. In this study, uniform and fine particles of about 19 nm were achieved via sol-gel combustion. The synthesized particles were consolidated by hot-pressing with at different sintering temperatures and the mid-IR transmittance reached 83.5 %, close to the theoretical transmittance, when sintered at 1,350 °C with 50 MPa. Ma et al. demonstrated the relationship between the optical transmittance and microstructure of a Y_2O_3-MgO nanocomposite with variations of the hot-pressing temperature.[101] As shown in Fig. 10, it was notable that a low sintering temperature resulted in degraded infrared transmittance owing to residual pores, which induced significant pore scattering. On the other hand, with increasing sintering temperature, the density and grain size of the Y_2O_3-MgO nanocomposite increased. The high density improved the mid-IR transmittance. The large grains increased the possibility of grain boundary scattering, which could limit the passing of incident light of short wavelength.

Sun et al. presented a kinetic analysis of Y_2O_3-MgO nanocomposite fabricated by microwave sintering.[103] They conducted the densification process of a Y_2O_3-MgO nanocomposite fabricated by both microwave and conventional sintering process. High density could be achieved with low grain growth activation energy when the nanocomposite was sintered by microwave sintering. Mathew et al. used a novel resistive coupled microwave sintering method to obtain higher density and finer domain size of a Y_2O_3-MgO nanocomposite than with the conventional microwave sintering process.[102] The sintered nanocomposite showed excellent infrared transmittance of 82.8 % at 5 μm of wavelength. In addition, it had high thermal conductivity of 20.55 Wm^{-1} K^{-1} at room temperature.

The synthesis of Y_2O_3-MgO nanoparticles is a decisive factor to achieve outstanding optical properties. The size and morphology of the synthesized particles closely determine the sinterability of the transparent ceramics. In this regard, many researchers have investigated the synthesis methods of Y_2O_3-MgO nanopowder including a flame pyrolysis technique[106] and sol-gel combustion methods.[58,100,104,105,107-112] The combustion method, in particular, is a novel technique to synthesize nanocomposite particles, where fine and high purity particles are fabricated quickly through a single ignition reaction. Notably, the size and morphology of the initial particles can be well-controlled by changing the stoichiometry of metal nitrate and fuel, including glycine, urea, and citric acid. The ratio has an effect on the flame temperature,

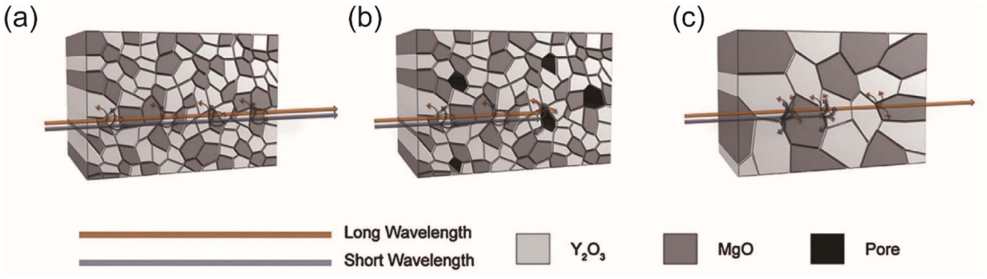

Fig. 10. Scheme of scattering mechanism of Y_2O_3-MgO nanocomposite with (a) fine grain and full density, (b) fine grain with large pores, (c) and large grain size with full density, Reproduced with permission from Ref.,[101] Copyright 2017, Elsevier.

which impacts the nucleation rate and exothermic decomposition reaction. The amount of evolved gases during the decomposition process inhibits the agglomeration of particles. Muoto et al. synthesized Y_2O_3-MgO nanoparticles by sol-gel combustion with different ratios of metal nitrate to ammonium acetate precursor.[113] They found that the density of the sintered specimens differed when using particles synthesized with different amounts of ammonium acetate. Ma et al. synthesized nanocomposite particles by the glycine nitrate process(GNP) with different stoichiometric ratios.[101] The synthesized particles exhibited fine size of 10 nm in the fuel sufficient system and showed the outstanding sinterability and optical transmittance close to the theoretical value. In addition, the hardness and thermal conductivity were also enhanced in the fuel rich system since the residual pores and grain growth could be well-controlled during the HP sintering process.

Severe agglomeration of the synthesized nanoparticles has a negative effect on the sintering behavior of Y_2O_3-MgO nanocomposite, there have been efforts to uniformly disperse the particles by an ultrasonic horn and ethanol floatation.[114] The treated particles form a homogeneous distribution and fine domain size, resulting in outstanding infrared transmittance after sintering.

Controlling the absorption peaks of Y_2O_3-MgO nanocomposite in the mid-infrared region is an important issue. An intense peak at 7 μm is assigned to intrinsic phonon absorption of Y_2O_3-MgO ceramics. When there are carbonate group residues after ceramic processing, asymmetrical and symmetrical stretching vibration of the carboxylate group affect this absorption peak significantly.[104] A weak absorption peak at 4.28 μm is associated with carbon dioxide in the atmosphere.[115] Since the MgO phase has a strong hydrophilic property, the absorption peak at 3.25 μm is ascribed to H_2O in the environment.[69]

3.3 $MgAl_2O_4$

$MgAl_2O_4$ spinel is a solid compound of MgO and Al_2O_3, and an inherently transparent material owing to its cubic crystal structure. It is considered a protective dome material for IR seeker, because of its good mechanical durability and high theoretical transmittance in the IR wavelength.[116] The light transmittance at the wavelength of interest is marginally superior to two competitive materials, AlON and sapphire. When the composition of spinel material is expressed as $MgO \cdot nAl_2O_3$, the n value has a wide range of 0.6-7.7. It is known that mechanical properties and light transmittance are influenced by the compositional change.

Sutorik et al. reported a noticeable difference in hardness values as the n value increases, that is, as the Al_2O_3 content increases.[117-119] The hardness value of n = 1.0 was 10 % higher than the hardness value of n = 2.5, and a similar trend for hardness values was also reported by Waetzig et al.[120] Krell et al. reported that the IR cut-off wavelength decreased with increasing Al_2O_3 content.[121] In the case of a low n value of what, the IR cut-off was about 6.5 μm, whereas for n = 2.5, the cut-off was observed at wavelengths lower than 6 μm. Therefore, excessive Al_2O_3 should be avoided since it lowers the transmittance of infrared rays as well as hardness.

The improvements in mechanical properties such as hardness and strength are important for the purposes of transparent windows and solid protection of IR sensors. Thus, there has been extensive researches to enhance mechanical properties by means of suppressing grain growth.[122-125] Recently, it has been reported that grain size can be controlled to less than several tens of nanometers by an extreme low temperature sintering method. Wollmershauser et al. used a multi-anvil device to produce transparent $MgAl_2O_4$ with 28 nm grain size at a pressure of 2 GPa at 800 °C.[126] The raw material particle size can be maintained even after sintering, resulting in a high hardness of 20 GPa, which is much higher than the typical hardness of spinel in the range of 13-16 GPa.[122] More recently, in 2016, Muche et al. produced a spinel with a grain size of less than 10 nm through a deformable punch SPS process and achieved a very high hardness of 28.4 GPa, and the hardness of the spinel was entirely proportional to the square root of the grain size.[127]

In order to produce transparent $MgAl_2O_4$ ceramics, the characteristics of the raw material powder such as purity and particle size distribution play a very important role. There have been reports of various impurities affecting the light transmittance of spinel. First, the formation of point defects or secondary phase precipitation by carbon deteriorates the light transmittance. Bernard-Granger et al. reported that when using the SPS process, amorphous carbon precipitates inside the $MgAl_2O_4$ ceramic, resulting in discoloration.[128] Goldstein reported that discoloration appears when transparent spinel is sintered using a graphite furnace, which is explained by the occurrence of oxygen vacancies inside the lattice of $MgAl_2O_4$ by the carbon reducing atmosphere.[80] When a HP process is used, a small amount of LiF sintering agent is usually added to produce transparent $MgAl_2O_4$. However, if the $LiAlO_2$ secondary phase generated during the sintering process is not removed, it acts as a light-scattering source, thereby significantly reducing the light transmittance.[129] It has been reported that the light transmittance varies depending on the purity of the initial powder, even when an identical manufacturing process is applied, as shown in Fig. 11. Reimanis et al. reported that the ultra-

Fig. 11. Transparent $MgAl_2O_4$ ceramics made from commercial powder(left) and acid-purified powder(right), Reproduced with permission from Ref.,[135] Copyright 2015, OSA publishing.

high-purity powder synthesized in the laboratory became a highly transparent ceramic, whereas the sintered ceramics from commercial $MgAl_2O_4$ powder containing impurities showed only translucency.[130] Villalobos et al. reported that significant enhancement of light transmittance could be achieved by acid-purification of the commercial spinel powder.[131]

The particle size and distribution of the initial powder also affect the transparency of the sintered body. Bonnefont et al. reported that SPS of three commercial powders with different particle size resulted in the transparency difference.[132] It has been reported that the particle size of the raw material influences the light transmittance in the reaction sintering of MgO-Al_2O_3. When the pore distribution of the green body is more uniform, the sinterability becomes better when using fine particles. However, the light transmittance showed the opposite tendency. it is higher for coarser raw particles.[121]

There has been intensive researches and development on two major applications for $MgAl_2O_4$[133] transparent bulletproof windows and transparent IR domes. The former is produced by Armorline, a US defense company, with a combined HP and HIP strategy. The production process for transparent spinel flat plate having a size of 1 m or more in length and width was developed. In the case of a transparent IR dome, TA&T succeeded in developing dome-shaped transparent spinel through a sinter-HIP process based on the Joint Common Missile(JCM, 2004~2007) and Joint Air-to-Ground Missile (JAGM, 2008~present) development program of the U.S. Army. In addition, various potential applications are under consideration, including spacecraft windows, multi-purpose windows for vehicles, small lenses for UV lithography, and so on.[134]

4. Summary and Conclusions

With remarkable advances in ceramic processing and sintering technologies, transparent polycrystalline ceramics for visible/IR windows have been developed. The ceramic processing includes determination of the powder size distribution, purity and sintering aids. The particle size and distribution affect the microstructure of green pellets. Among the light scattering sources, residual pores in ceramics fatally hinder a optical transmittance. The control of the grain growth kinetics is key technology to eliminate pores sufficiently during the sintering process. Achieving high mechanical strength is also an important issue for visible/IR windows to be used in harsh environments. Transparent ceramics with fine grain microstructure are desired to enhance the mechanical strength and hardness. Yttria-based IR transparent ceramics and $MgAl_2O_4$ spinel are promising candidates for future window applications.

Acknowledgements

This work was supported by the Materials & Components Technology Development(MCTD) Program(Project no. 10047010) funded by the Ministry of Trade, Industry & Energy(MOTIE) of Korea.

References

1. W. Kim, G. Villalobos, C. Baker, J. Frantz, B. Shaw, S. Bayya, B. Sadowski, M. Hunt, I. Aggarwal and J. Sanghera, Opt. Eng., **52**, 21003 (2012).
2. A. Krell, J. Klimke and T. Hutzler, Opt. Mater., **31**, 1144 (2009).
3. M. E. Thomas, R. I. Joseph and W. J. Tropf, Appl. Opt., **27**, 239 (1988).
4. S. F. Wang, J. Zhang, D. W. Luo, F. Gu, D. Y. Tang, Z. L. Dong, G. E. B. Tan, W. X. Que, T. S. Zhang, S. Li and L. B. Kong, Prog. Solid State Chem., **41**, 20 (2013).
5. P. Hogan, T. Stefanik, C. Willingham, R. Gentilman, R. Integrated, D. Systems, 10th DoD Electromagn. Wind. Symp., Norfolk, VA (2004).
6. D. C. Harris, Infrared Phys. Technol. **39**, 185 (1998).
7. B. D. William and W. Chen, J. Am. Ceram. Soc., **76**, 2086 (1993).
8. R. Apetz and M. P. B. Van Bruggen, J. Am. Ceram. Soc., **86**, 480 (2003).
9. A. Krell, T. Hutzler, J. Klimke, J. Eur. Ceram. Soc. **29** 207 (2009).
10. Y. Kodera, C. L. Hardin and J. E. Garay, Scr. Mater., **69**, 149 (2013).
11. Z. M. Seeley, J. D. Kuntz, N. J. Cherepy and S. A. Payne, Opt. Mater., **33**, 1721 (2011).

12. P. Chen and I. Chen, J. Am. Ceram. Soc., **79**, 1801 (1996).
13. D. C. Harris, L. R. Cambrea, L. F. Johnson, R. T. Seaver, M. Baronowski, R. Gentilman, C. Scott Nordahl, T. Gattuso, S. Silberstein, P. Rogan, T. Hartnett, B. Zelinski, W. Sunne, E. Fest, W. Howard Poisl, C. B. Willingham, G. Turri, C. Warren, M. Bass, D. E. Zelmon and S. M. Goodrich, J. Am. Ceram. Soc., **96**, 3828 (2013).
14. T. Kim, D. Kim and S. Kang, J. Alloys Compd., **587**, 594 (2014).
15. K. Ksukuma, J. Ceram. Soc. Japan, **114**, 802 (2006).
16. I. Reimanis and H. J. Kleebe, J. Am. Ceram. Soc., **92**, 1472 (2009).
17. J. Sanghera, S. Bayya, G. Villalobos, W. Kim, J. Frantz, B. Shaw, B. Sadowski, R. Miklos, C. Baker, M. Hunt, I. Aggarwal, F. Kung, D. Reicher, S. Peplinski, A. Ogloza, P. Langston, C. Lamar, P. Varmette, M. Dubinskiy and L. Desandre, Opt. Mater., **33**, 511 (2011).
18. W. Kim, C. Baker, G. Villalobos, S. Bayya, M. Hunt, B. Sadowski, I. Aggarwal and J. Sanghera, Wind. Dome Technol. Mater. XIV., **9453**, 945303 (2015).
19. S. Bayya, G. Villalobos, W. Kim, J. Sanghera, G. Chin, M. Hunt, B. Sadowski, F. Miklos and I. Aggarwal, Proc. SPIE **8837**, 88370V (2013).
20. L. Wen, X. Sun, Q. Lu, G. Xu and X. Hu, Opt. Mater., **29**, 239 (2006).
21. Y. Wu, J. Du and R. L. Clark, Mater. Lett., **107**, 68 (2013).
22. N. Saito, S. Matsuda and T. Ikegami, J. Am. Ceram. Soc., **81**, 2023 (1998).
23. N. A. Dulina, Y. V. Yermolayeva, A. V. Tolmachev, Z. P. Sergienko, O. M. Vovk, E. A. Vovk, N. A. Matveevskaya and P. V. Mateychenko, J. Eur. Ceram. Soc., **30**, 1717 (2010).
24. Y. Huang, D. Jiang, J. Zhang, Q. Lin and Z. Huang, Ceram. Int., **37**, 3523 (2011).
25. J. Sanghera, W. Kim, G. Villalobos, C. Baker, J. Frantz, B. Shaw, S. Bayya, B. Sadowski, M. Hunt and I. Aggarwal, Proc. SPIE **8039**, 803903 (2011).
26. X. Xu, X. Sun, H. Liu, J.G. Li, X. Li, D. Huo and S. Liu, J. Am. Ceram. Soc., **95**, 3821 (2012).
27. X. Qin, H. Yang, G. Zhou, D. Luo, J. Zhang, S. Wang and J. Ma, Mater. Res. Bull., **46**, 170 (2011).
28. D. Sordelet and M. Akinc, J. Am. Ceram. Soc., **71**, 1148 (1988).
29. S. Satapathy, A. Ahlawat, A. Paliwal, R. Singh, M. K. Singh and P. K. Gupta, Cryst. Eng. Commun., **16**, 2723 (2014).
30. W. K. Jung, H. J. Ma, S. W. Jung and D. K. Kim, J. Am. Ceram. Soc., **100**, 1876 (2017).
31. V. V. Osipov, K. E. Luk'yashina, V. I. Solomonov, V. A. Shitov, A. N. Orlov, V. V. Platonov and A. V. Spirin, Bull. Lebedev Phys. Inst., **36**, 347 (2009).
32. X. Hou, S. Zhou, W. Li and Y. Li, J. Eur. Ceram. Soc., **30**, 3125 (2010).
33. X. Hou, S. Zhou, Y. Li and W. Li, Opt. Mater., **32**, 920 (2010).
34. L. Jin, G. Zhou, S. Shimai, J. Zhang and S. Wang, J. Eur. Ceram. Soc., **30**, 2139 (2010).
35. Q. Yi, S. Zhou, H. Teng, H. Lin, X. Hou and T. Jia, J. Eur. Ceram. Soc., **32**, 381 (2012).
36. G. Busker, A. Chroneos, R. W. Grimes and I.-W. Chen, J. Am. Ceram. Soc., **82**, 1553 (1999).
37. K. Rozenburg, I. E. Reimanis, H.-J. Kleebe and R. L. Cook, J. Am. Ceram. Soc., **91**, 444 (2008).
38. R. Naghizadeh, H. R. Rezaie and F. Golestani-Fard, Ceram. Int., **37**, 349 (2011).
39. J. Aguilar, A. Arato, M. Hinojosa and U. Ortiz, Mater. Sci. Forum, **442**, 79 (2003).
40. J. M. Kim, H. N. Kim, Y. J. Park, J. W. Ko, J. W. Lee and H. D. Kim, J. Eur. Ceram. Soc., **36**, 2027 (2015).
41. G. Bernard-Granger, C. Guizard and A. Addad, J. Am. Ceram. Soc., **91**, 1703 (2008).
42. P. Zhang, P. Liu, Y. Sun, X. Peng, Z. Wang, S. Wang and J. Zhang, J. Alloys Compd., **657**, 246 (2016).
43. G. Bernard-Granger, C. Guizard and L. San-Miguel, J. Am. Ceram. Soc., **90**, 2698 (2007).
44. P. Zhang, P. Liu, Y. Sun, J. Wang, Z. Wang, S. Wang and J. Zhang, J. Alloys Compd., **646**, 833 (2015).
45. H. Shahbazi, H. Shokrollahi and M. Tataei, Ceram. Int., **44**, 8725 (2018).
46. H. Choi, S. Yong and D. K. Kim, **50**, 434 (2013).
47. J. M. Kim, H. N. Kim, Y. J. Park, J. W. Ko, J. W. Lee, H. D. Kim, Ceram. Int., **41**, 13354 (2015).
48. Y. Huang, D. Jiang, J. Zhang, Q. Lin and Z. Huang, J. Am. Ceram. Soc., **93**, 2964 (2010).
49. Y. Wang, B. Lu, X. Sun, T. Sun and H. Xu, Adv. Appl. Ceram., **110**, 95 (2011).
50. T. Yanagida, Y. Fujimoto, S. Kurosawa, K. Watanabe, H. Yagi, T. Yanagitani, V. Jary, Y. Futami, Y. Yokota, A. Yoshikawa, A. Uritani, T. Iguchi and M. Nikl, Appl. Phys. Express, **4**, 2 (2011).
51. L. L. Zhu, Y. J. Park, L. Gan, S. Il. Go, H. N. Kim, J. M. Kim, J. W. Ko, Q. Yi, S. Zhou, H. Teng, H. Lin, X. Hou and T. Jia, Ceram. Int., **43**, 8525 (2017).
52. X. Li, X. Mao, M. Feng, J. Xie, B. Jiang and L. Zhang, J. Eur. Ceram. Soc., **36**, 4181 (2016).
53. W. Zhang, T. Lu, N. Wei, B. Ma, F. Li, Z. Lu and J. Qi, Opt. Mater., **34**, 685 (2012).
54. C. Ma, F. Tang, J. Zhu, M. Du, X. Yuan, Y. Yu, K. Wang, Z. Wen, J. Zhang, J. Long, W. Guo and Y. Cao, J. Am. Ceram. Soc., **6**, 1 (2016).
55. W. Zhang, T. Lu, B. Ma, N. Wei, Z. Lu, F. Li, Y. Guan, X. Chen, W. Liu and L. Qi, Opt. Mater., **35**, 2405 (2013).
56. L. Gan, Y.J. Park, H. Kim, J.M. Kim, J.W. Ko, and J.W. Lee, Ceram. Int., **41**, 9622 (2015).
57. L. Gan, Y.-J. Park, M.-J. Park, H. Kim, J.-M. Kim, J.-

W. Ko and J.-W. Lee, J. Am. Ceram. Soc., **98**, 2002 (2015).
58. S. Xu, J. Li, C. Li, Y. Pan and J. Guo, J. Am. Ceram. Soc., **98**, 1019 (2015).
59. M. R. du Merac, I. E. Reimanis, C. Smith, H. J. Kleebe, M. M. Müller, Int. J. Appl. Ceram. Technol., **10**, E33 (2013).
60. L. Gan, Y. Park, H. Kim, J. Kim, J. Ko and J. Lee, J. Eur. Ceram. Soc. Ceram. Soc., **36**, 911 (2016).
61. H. J. Ma, W. K. Jung, C. Baek and D. K. Kim, J. Eur. Ceram. Soc., **37**, 4902 (2017).
62. W. Luo, Y. Pan, C. Li, H. Kou and J. Li, J. Alloys Compd., **724**, 45 (2017).
63. W. Luo, R. Xie, M. Ivanov, Y. Pan and H. Kou, J. Li, Ceram. Int., **43**, 6891 (2017).
64. O. Guillon, J. Gonzalez-Julian, B. Dargatz, T. Kessel, G. Schierning, J. Räthel and M. Herrmann, Adv. Eng. Mater., **16**, 830 (2014).
65. U. Anselmi-Tamburini, J. N. Woolman and Z. A. Munir, Adv. Funct. Mater., **17**, 3267 (2007).
66. J. Klimke, M. Trunec and A. Krell, J. Am. Ceram. Soc., **94**, 1850 (2011).
67. K. Morita, B.N. Kim, H. Yoshida, K. Hiraga and Y. Sakka, J. Eur. Ceram. Soc., **36**, 2961 (2016).
68. K. Morita, B.-N. Kim, H. Yoshida, K. Hiraga and Y. Sakka, Acta Mater., **84**, 9 (2015).
69. D. Jiang and A. K. Mukherjee, J. Am. Ceram. Soc., **93**, 769 (2010).
70. Y. Futami, T. Yanagida, Y. Fujimoto, J. Pejchal, M. Sugiyama, S. Kurosawa, Y. Yokota, A. Ito, A. Yoshikawa and T. Goto, Radiat. Meas., **55**, 136 (2013).
71. K. Morita, B.N. Kim, H. Yoshida, K. Hiraga and Y. Sakka, J. Am. Ceram. Soc., **98**, 378 (2015).
72. F. Tang, Y. Cao, J. Huang, H. Liu, W. Guo and W. Wang, J. Am. Ceram. Soc., **95**, 56 (2012).
73. J. Sanghera, W. Kim, G. Villalobos, B. Shaw, C. Baker, J. Frantz, B. Sadowski and I. Aggarwal, Materials, **5**, 258 (2012).
74. Z. Wang, L. Zhang, H. Yang, J. Zhang, L. Wang and Q. Zhang, Ceram. Int., **42**, 4238 (2016).
75. K. Serivalsatit, B. Y. Kokuoz, B. Kokuoz and J. Ballato, Opt. Lett., **34**, 1033 (2009).
76. K. Serivalsatit and J. Ballato, J. Am. Ceram. Soc., **93**, 3657 (2010).
77. W. Li, S. Zhou, H. Lin, H. Teng, N. Liu, Y. Li, X. Hou and T. Jia, J. Am. Ceram. Soc., **93**, 3819 (2010).
78. K. Tsukuma, I. Yamashita and T. Kusunose, J. Am. Ceram. Soc., **91**, 813 (2008).
79. A. Goldstein, A. Goldenberg and M. Hefetz, J. Ceram. Soc. Japan, **117**, 1281 (2009).
80. A. Goldstein, J. Eur. Ceram. Soc., **32**, 2869 (2012).
81. R. P. Yavetskiy, V. N. Baumer, M. I. Danylenko, A. G. Doroshenko, I. N. Ogorodnikov, I. A. Petrusha, A. V. Tolmachev and V. Z. Turkevich, Ceram. Int., **40**, 3561 (2014).
82. Y. K. Kim, H. K. Kim, D. K. Kim and G. Cho, J. Mater. Res., **19**, 413 (2004).
83. Y. K. Kim, H. K. Kim, G. Cho and D. K. Kim, Nucl. Instrum. Methods Phys. Res., Sect. B, **225**, 392 (2004).
84. J. He, X. Li, S. Liu, Q. Zhu, J.-G. Li and X. Sun, J. Eur. Ceram. Soc., **35**, 2369 (2015).
85. H. Qin, H. Liu, Y. Sang, Y. Lv, X. Zhang, Y. Zhang, T. Ohachi and J. Wang, CrystEngComm, **14**, 1783 (2012).
86. W. H. Rhodes, J. Am. Ceram. Soc., **64**, 13 (1981).
87. K. Majima, N. Niimi, M. Watanabe, S. Katsuyama and H. Nagai, J. Alloys Compd., **193**, 280 (1993).
88. J. A. Harrington, C. Greskovich, J. Appl. Phys., **48**, 1585 (1977).
89. A. Ikesue, K. Kamata and K. Yoshida, J. Am. Ceram. Soc., **79**, 359 (1996).
90. G. Toda and I. Matsuyama, J. Japan Soc. Powder Powder Metall., **35**, 486 (1988).
91. V. V. Osipov, V. A. Shitov, R. N. Maksimov and V. I. Solomonov, Opt. Mater., **50**, 65 (2015).
92. V. V. Osipov, V. I. Solomonov, V. A. Shitov, R. N. Maksimov, A. N. Orlov and A. M. Murzakaev, Russ. Phys. J., **58**, 107 (2015).
93. J. Zhang, L. An, M. Liu, S. Shimai and S. Wang, J. Eur. Ceram. Soc., **29**, 305 (2009).
94. K. Serivalsatit, B. Kokuoz, B. Yazgan-Kokuoz, M. Kennedy and J. Ballato, J. Am. Ceram. Soc., **93**, 1320 (2010).
95. M. Kodo, K. Soga, H. Yoshida and T. Yamamoto, J. Eur. Ceram. Soc., **30**, 2741 (2010).
96. H. Yoshida, K. Morita, B. N. Kim, K. Soga and T. Yamamoto, J. Eur. Ceram. Soc., **38**, 1972 (2018).
97. W. K. Jung, H. J. Ma, Y. Park, D. K. Kim, Scr. Mater., **137**, 1 (2017).
98. B. H. Kear, R. Sadangi, V. Shukla, T. Stefanik, and R. Gentilman, Proc. SPIE **5786**, 227 (2005).
99. L. Huang, W. Yao, J. Liu, A. K. Mukherjee and J. M. Schoenung, Scr. Mater., **75**, 18 (2014).
100. S. Xu, J. Li, H. Kou, Y. Shi, Y. Pan and J. Guo, Ceram. Int., **41**, 3312 (2015).
101. H. J. Ma, W. K. Jung, C. Baek and D. K. Kim, J. Eur. Ceram. Soc., **37**, 4902 (2017).
102. M. C.T., J.K. Thomas, S. Y.V., J. Koshy, and S. Solomon, Ceram. Int., **43**, 17048 (2017).
103. H. Sun, Y. Zhang, H. Gong, T. Li and Q. Li, Ceram. Int., **40**, 10211 (2014).
104. J. Wang, D. Chen, E. H. Jordan and M. Gell, J. Am. Ceram. Soc., **93**, 3535 (2010).
105. S. Xu, J. Li, C. Li, Y. Pan and J. Guo, J. Am. Ceram. Soc., **98**, 2796 (2015).
106. T. Stefanik, R. Gentilman, P. Hogan, Wind. Dome Technol. Mater. X, in: Proc. SPIE 6545 (2007).
107. J. Wang, E. H. Jordan and M. Gell, J. Therm. Spray Technol., **19**, 873 (2010).
108. C. K. Muoto, E. H. Jordan, M. Gell, M. Aindow, J. Am. Ceram. Soc., **94**, 372 (2011).

109. A. Iyer, J. K. M. Garofano, J. Reutenaur, S. L. Suib, M. Aindow, M. Gell and E. H. Jordan, J. Am. Ceram. Soc., **96**, 346 (2013).
110. C.-H. Chen, J. K. M. Garofano, C. K. Muoto, A. L. Mercado, S. L. Suib, M. Aindow, M. Gell and E. H. Jordan, J. Am. Ceram. Soc., **94**, 367 (2011).
111. A. Alhaji, R. S. Razavi, A. Ghasemi, M. R. Loghman-Estarki, Ceram. Int., **43**, 2541 (2017).
112. D. Jiang, A. K. Mukherjee, Proc. SPIE **7030**, 703007 (2008).
113. C. K. Muoto, E. H. Jordan, M. Gell, M. Aindow, J. Am. Ceram. Soc., **94**, 4207 (2011).
114. J. Liu, W. Yao, B. Kear and A. K. Mukherjee, Mater. Sci. Eng., B, **171**, 149 (2010).
115. D. Jiang, A. K. Mukherjee, Scr. Mater., **64**, 1095 (2011).
116. A. A. DiGiovanni, L. Fehrenbacher, D. W. Roy, Proc. SPIE 5786, Wind. Dome Technol. Mater. IX, **5786**, 56 (2005).
117. A. C. Sutorik, C. Cooper and G. Gilde, J. Am. Ceram. Soc., **96**, 3704 (2013).
118. A. C. Sutorik, G. Gilde, J. J. Swab, C. Cooper, R. Gamble and E. Shanholtz, J. Am. Ceram. Soc., **95**, 636 (2012).
119. A. C. Sutorik, G. Gilde, C. Cooper, J. Wright and C. Hilton, J. Am. Ceram. Soc., **95**, 1807 (2012).
120. K. Waetzig and A. Krell, J. Am. Ceram. Soc., **99**, 946 (2016).
121. A. Krell, K. Waetzig and J. Klimke, J. Eur. Ceram. Soc., **32**, 2887 (2012).
122. A. Krell and A. Bales, Int. J. Appl. Ceram. Technol., **8**, 1108 (2011).
123. T. Mroz, L. M. Goldman, A. D. Gledhill, D. Li and N. P. Padture, Int. J. Appl. Ceram. Technol., **9**, 83 (2012).
124. K. Morita, B. N. Kim, H. Yoshida and K. Hiraga, J. Am. Ceram. Soc., **92**, 1208 (2009).
125. A. Rothman, S. Kalabukhov, N. Sverdlov, M. P. Dariel and N. Frage, Int. J. Appl. Ceram. Technol., **11**, 146 (2014).
126. J. A. Wollmershauser, B. N. Feigelson, E. P. Gorzkowski, C. T. Ellis, R. Goswami, S. B. Qadri, J. G. Tischler, F. J. Kub and R. K. Everett, Acta Mater., **69**, 9 (2014).
127. D. N. F. Muche, J. W. Drazin, J. Mardinly, S. Dey and R. H. R. Castro, Mater. Lett., **186**, 298 (2017).
128. G. Bernard-Granger, N. Benameur, C. Guizard and M. Nygren, Scr. Mater. **60**, 164 (2009).
129. K. K. Rozenburg, I. E. Reimanis, H. J. Kleebe and R. L. Cook, J. Am. Ceram. Soc., **90**, 2038 (2007).
130. I. E. Reimanis, H.-J. Kleebe, R. L. Cook and A. DiGiovanni, Def. Secur. Symp. (2004).
131. G. Villalobos, S. Bayya, W. Kim, C. Baker, J. Sanghera, M. Hunt, B. Sadowski, F. Miklos and I. Aggarwal, J. Mater. Res., **29**, 2266 (2014).
132. G. Bonnefont, G. Fantozzi, S. Trombert and L. Bonneau, Ceram. Int., **38**, 131 (2012).
133. A .A. DiGiovanni, A. LaRoche, L. Schubel, L. Fehrenbacher, D. W. Roy, Proc. SPIE 6545, Wind. Dome Technol. Mater. X, **6545**, 654514 (2007).
134. M. Rubat Du Merac, H. J. Kleebe, M. M. Müller and I. E. Reimanis, J. Am. Ceram. Soc., **96**, 3341 (2013).
135. W. Kim, G. Villalobos, C. Baker, J. Frantz, B. Shaw, S. Bayya, B. Sadowski, M. Hunt, B. Rock, I. Aggarwal and J. Sanghera, Appl. Opt., **54**, F210 (2015).